Title
Fusion by earthquake fault friction: Stick or slip?

Journal
Journal of Geophysical Research-Solid Earth, 110(B12)

ISSN
0148-0227

Authors
Fialko, Y
Khazan, Y

Publication Date
2005-12-01

Peer reviewed

J. Geophys. Res., *110*, doi:10.1029/2005JB003869, 2005

Fusion by earthquake fault friction: Stick or slip?

Yuri Fialko and Yakov Khazan

Institute of Geophysics and Planetary Physics, Scripps Institution of Oceanography, University of California San Diego, La Jolla, California

Abstract. Field observations of pseudotachylites, and experimental studies of high-speed friction indicate that melting on a slipping interface may significantly affect the magnitude of shear stresses resisting slip. We investigate the effects of rock melting on the dynamic friction using theoretical models of shear heating that couple heat transfer, thermodynamics of phase transitions, and fluid mechanics. Results of laboratory experiments conducted at high (order of m/s) slip velocities but low (order of MPa) normal stresses suggest that the onset of frictional melting may give rise to substantial increases in the effective fault strength, presumably due to viscous effects. However, extrapolation of the modeling results to in situ conditions suggests that the efficiency of viscous braking is significantly reduced under high normal and shear stresses. When transient increases in the dynamic fault strength due to fusion are not sufficient to inhibit slip, decreases in the effective melt viscosity due to shear heating and melting of clasts drastically decrease the dynamic friction, resulting in a nearly complete stress drop ("thermal runaway"). The amount of energy dissipation associated with the formation of pseudotachylites is governed by the temperature dependence of melt viscosity, and the average clast size in the fault gouge prior to melting. Clasts from a coarse-grained gouge have lower chances of survival in a pseudotachylite due to a higher likelihood of non-equilibrium overheating. The maximum temperature and energy dissipation attainable on the fault surface are ultimately limited by either the rock solidus (via viscous braking, and slip arrest), or liquidus (via thermal runaway, and vanishing resistance to sliding). Our modeling results indicate that the thermally-activated fault strengthening and rupture arrest are unlikely to occur in most mafic protoliths, but might be relevant for quartz-rich rocks, especially at shallow (< 5-7 km) depths where the driving shear stress is relatively low.

1. Introduction

It is generally believed that increases in temperature during slip on earthquake faults may dramatically affect the frictional properties of rocks in the earthquake fault zone, and the dynamic fault strength [*Sibson*, 1975; *Lachenbruch*, 1980; *Kanamori and Heaton*, 2000]. Thermally-activated mechanisms that may affect the fault resistance to shear include thermal pressurization [*Sibson*, 1973; *Lachenbruch*, 1980; *Mase and Smith*, 1987], frictional melting [*Jeffreys*, 1942; *McKenzie and Brune*, 1972; *Sibson*, 1975; *Maddock*, 1986], and flash heating of fault asperities [*Rice*, 1999]. However, the magnitude, the spatio-temporal patterns, and even the sign of the thermally-induced variations in the effective fault friction are poorly known. Theoretical models predict temperature increases in excess of the host rock solidus even for moderate seismic slip (∼1 m) and low fault friction (e.g., <20 MPa, sufficient to satisfy the "heat flow paradox" of the San Andreas fault [*Brune*

et al., 1969; *Lachenbruch and Sass*, 1980]) if the width of a slipping region is of the order of centimeters or less [e.g., *Jeffreys*, 1942; *Cardwell et al.*, 1978; *Fialko*, 2004a]. Such narrow slip zones are sometimes observed in the field [e.g., *Chester and Chester*, 1998; *Sibson*, 2003; *Suppe*, 1985, p.285]. Although large crustal faults may be associated with significantly thicker ($1-10^3$ m), and possibly scale-dependent "damage" zones [*Scholz*, 1990; *Fialko et al.*, 2002; *Fialko*, 2004b], it is conceivable that the latter represent cumulative inelastic deformation due to many generations of seismic events, rather than the characteristic thickness of a slip zone involved in individual earthquakes. Field observations of pseudotachylites (glassy veins of dark aphanitic rock in cores of the exposed fault zones) are direct evidence that the co-seismic frictional heating may be sufficiently robust to raise the average fault temperature above solidus [*Philpotts*, 1964; *Price*, 1970; *Wallace*, 1976; *Swanson*, 1992; *Wenk et al.*, 2000]. While it is still debated whether the fault zone melting is a rare phenomenon, it is clear that at least in some cases the physics governing the fault resistance to slip undergoes a dramatic change from the "dry" friction dominated by the asperity contacts, to the viscous shear (Couette flow). Such a transition may potentially provide a great deal of information about the absolute stress acting on an earthquake rupture, and seismic efficiency. Recovering such information requires insights into the effects of melting on the dynamic fault strength.

It is usually assumed that the frictionally generated melt is likely to result in the marked fault weakening - for instance, if viscous stresses associated with shearing of the melt film are smaller than frictional stresses prior to melting [*McKenzie and Brune*, 1972], if patches of melt dynamically support some fraction of the fault-normal stress [*Brodsky and Kanamori*, 2001], or if the local heating of micro-asperities on the slip interface reduces the effective strength of the asperities ("flash melting") [*Rice*, 1999]. At the same time, theoretical arguments suggest that stresses associated with shearing of thin layers of melt may not be small, especially at the onset of melting and for silicic melt compositions [*Scholz*, 1990; *Fialko*, 2004a]. High-speed friction experiments reveal a complex non-monotonic behavior of the dynamic shear strength, with a pronounced peak of shear resistance at the onset of macroscopic melting [*Tsutsumi and Shimamoto*, 1997; *Hirose and Shimamoto*, 2003]. While the these results appear to be consistent with the viscous nature of transient strengthening during the development of a continuous melt layer [*Fialko*, 2004a; *Hirose and Shimamoto*, 2005], there is still no consensus about implications from the laboratory data for the earthquake rupture dynamics [e.g., *Koizumi et al.*, 2004; *Spray*, 2005]. In particular, high-speed friction experiments of *Tsutsumi and Shimamoto* [1997] and *Hirose and Shimamoto* [2003] were conducted at low (2-3 MPa) normal stresses. Because the resistance to slip in the viscous regime only weakly (if at all) depends on the normal stress, the apparent coefficient of friction has little physical meaning in the post-melting stage, and large values of the coefficient of friction reported at the onset of melting in low-pressure experiments may not be expected at larger normal stresses. In fact, the effective coefficient of friction associated with melting is predicted to nearly linearly decrease with an increasing normal stress (the actual dependence may be somewhat weaker than the inverse proportionality due to enhanced squeezing of melt out of the slip interface at higher normal stresses, resulting in a thinner melt layer). In the absence of direct experimental measurements at high slip velocities and high normal stresses, the effect of melting on the effective shear strength of the slip interface may be investigated using numerical models.

Another important yet poorly understood problem that lends itself to a numerical treatment concerns the kinetics of post-melting weakening of the slip zone. Such weakening is expected to occur due to increases in the melt temperature, or decreases in the volume fraction of solid inclusions. A strong dependence of the melt viscosity on temperature and clast content implies a highly non-linear coupling between the slip velocity, viscous shear stresses, shear heating, and melting at the solid-liquid interface, both internal (e.g., on the clast boundaries) and external (between the melt and the host rocks). Obviously, post-melting decreases in the fault strength may be important for the dynamics of earthquake rupture only if the thermally-activated changes in melt rheology occur on time scales that are small compared to the typical rise times of earthquakes. In this paper we investigate the fluid-mechanical and thermodynamic aspects of frictional melting, and its implications and consequences for the dynamics of seismic slip.

2. Preliminaries: Shear heating of an Arrhenius liquid

We begin by considering the temporal evolution of temperature and stress associated with shearing of a layer of melt having a constant thickness $2w$, and an

Arrhenius-type rheology,

$$\eta(T) = A \exp\left(\frac{B}{T}\right), \tag{1}$$

where η is the dynamic viscosity of melt, T is the absolute temperature, and A and B are empirical constants that may be interpreted as the reference viscosity and activation temperature (ratio of activation energy to the universal gas constant), respectively. Theoretical arguments supported by a large amount of experimental data indicate that equation (1) adequately describes the temperature dependence of viscosity for most silicate melts [e.g., *Shaw*, 1972; *Dingwell*, 1998]. Shearing of a melt layer results in viscous dissipation, whereby the work done by the applied shear stress τ is converted into heat. The rate of heat generation by viscous dissipation is $\tau\partial\epsilon/\partial t$, where $\partial\epsilon/\partial t$ is the local strain rate in the fluid. Temperature variations across the melt layer are governed by a balance between shear heating of melt, and conductive heat loss from the melt to the ambient rocks. Because the thickness of the melt layer is small compared to any other characteristic length scale in the problem (e.g., the rupture size, or the amount of slip), the temperature evolution in the melt layer is well approximated by one-dimensional heat conduction,

$$\frac{\partial T}{\partial t} = \kappa\frac{\partial^2 T}{\partial x^2} + \frac{\tau}{c\rho}\frac{\partial \epsilon}{\partial t}, \text{ for } t > 0, |x| < w \tag{2}$$

where t is time, κ is the thermal diffusivity (for simplicity, assumed to be constant in this Section), c is the specific heat, ρ is the melt density, and x is the across-flow coordinate with the origin in the middle of the layer. The problem is closed by the Navier-Stokes constitutive relationship postulating a linear dependence between the applied stress and the resulting rate of shear strain,

$$\tau = \eta\frac{\partial \epsilon}{\partial t}. \tag{3}$$

In general, the heat exchange between the melt and the host rocks results in melting or solidification at the solid-liquid interface, so that the thickness of the melt layer may vary. In order to get a further analytical insight into the coupling between the thermal and fluid-mechanical parts of the problem, we defer the consideration of phase changes until Section 3, and assume that $w = \text{const}$. This assumption may be valid, e.g., if the velocity of melting/freezing at the melt-solid boundary is much less than w/t_s, where t_s is the rise time of seismic slip. Note that the formation of a melt layer having a finite thickness may occur nearly instantaneously if the thickness of the slip zone is larger than the characteristic length scale for thermal diffusion (i.e., the frictional heat generation is essentially adiabatic) [*Cardwell et al.*, 1978; *Fialko*, 2004a]. Let us now assume that melting of the slip zone occurs at temperature T_m, corresponding to both liquidus and solidus of the host rocks. It is instructive to consider the thermomechanical evolution of the melt layer under two types of boundary conditions, a constant applied shear stress τ_c, and a constant velocity of shearing V_c. The constant stress boundary condition may be more relevant for the initial stages of melting, immediately after a transition from the Coulomb friction to the viscous regime. In this case, τ_c represents the absolute shear stress resolved on the fault surface. The constant velocity boundary condition may be appropriate for later stages of slip, when the frictionally generated heat has substantially reduced the fault strength, so that the slip velocity is limited by the elastodynamics of rupture, rather than the melt viscosity.

2.1. Shear under constant stress, and conditions for thermal runaway

First, we consider viscous heating associated with shearing of the melt layer under a constant driving stress τ_c. Dimensional analysis of equation (2) suggests the following non-dimensional variables:

$$\begin{aligned} \text{non-dimensional across-flow coordinate} \quad \bar{x} &= \frac{x}{w}, \\ \text{non-dimensional time} \quad \bar{t} &= \frac{\kappa t}{w^2}, \\ \text{non-dimensional temperature} \quad \theta &= \frac{(T - T_m)B}{T_m^2}. \end{aligned} \tag{4}$$

Upon non-dimensionalization using (4), equation (2) becomes

$$\frac{\partial \theta}{\partial \bar{t}} = \frac{\partial^2 \theta}{\partial \bar{x}^2} + \text{Gn} \exp\left(-\frac{1}{\psi(\psi\theta + 1)}\right), \text{ for } t > 0, |\bar{x}| < 1 \tag{5}$$

where $\psi = T_m/B$, and Gn is the Gruntfest number that characterizes the ratio of heat generated by viscous dissipation to the conductive heat loss,

$$\text{Gn} = \frac{(\tau_c w)^2 B}{k A T_m^2}. \tag{6}$$

In equation (6), $k = c\rho\kappa$ is the thermal conductivity. Equation (5) can be readily solved (e.g., numerically) subject to boundary conditions

$$\theta = 0 \text{ for } |\bar{x}| = 1, \tag{7}$$

$$\frac{\partial \theta}{\partial \bar{x}} = 0 \text{ for } \bar{x} = 0, \tag{8}$$

and initial condition

$$\theta(\bar{x}) = 0 \text{ for } \bar{t} = 0. \tag{9}$$

Of particular interest is the case of adiabatic heating, when the heat conduction (first term on the right-hand side of equation (5)) is negligible compared to viscous dissipation (second term on the right-hand side of equation (5)). A simple analytical insight into the qualitative behavior of the adiabatic solution is allowed for the Frank-Kamenetzky approximation of the temperature dependence of melt rheology,

$$\eta(T) \approx A \exp\left(\frac{2B}{T_m}\right) \exp\left(-\frac{BT}{T_m^2}\right) = A \exp\left(\frac{1}{\psi} - \theta\right). \tag{10}$$

Equation (10) is obtained by linearizing the argument in the Arrhenius law (1) using a Taylor series expansion about the initial temperature T_m. Under these assumptions equation (5) is reduced to

$$\frac{\partial \theta}{\partial \bar{t}} = \mathrm{Gn}^* e^{\theta}, \tag{11}$$

where Gn^* is the modified Gruntfest number,

$$\mathrm{Gn}^* = \frac{(\tau_c w)^2 B}{k A T_m^2 e^{B/T_m}}. \tag{12}$$

Adiabatic conditions correspond to $\mathrm{Gn}^* \gg 1$. Integration of equation (11) with the initial condition (9) yields

$$\theta = -\log(1 - \mathrm{Gn}^* \bar{t}). \tag{13}$$

A bounded solution to equation (13) exists only for $\bar{t} < 1/\mathrm{Gn}^*$, implying a characteristic time scale

$$t_c = \frac{A \rho c T_m^2 e^{B/T_m}}{B \tau_c^2}, \tag{14}$$

that corresponds to the so-called thermal runaway (unlimited acceleration and heating of the melt layer) [*Gruntfest et al.*, 1964; *Yuen et al.*, 1978; *Fleitout and Froidevaux*, 1980]. A more general solution using the Arrhenius rheology (1) exhibits a similar step-like increase in temperature around time t_c, followed by a more gradual increase in the post-runaway phase. The details of temperature variations after the onset of thermal runaway are not relevant for geophysical applications because of unrealistically high slip velocities. Figure 1 shows the critical time t_c, as predicted by equation (14), for typical melt rheologies corresponding to "basaltic" and "granitic" compositions [*Shaw*, 1972; *McBirney*, 1993]. Numerical simulations accounting for the conductive heat loss and phase transitions indicate

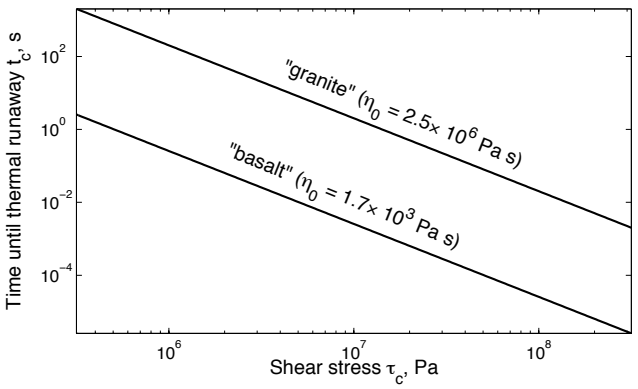

Figure 1. Characteristic evolution time between the onset of melting and the onset of thermal runaway for an adiabatic shear under a constant stress. "Basaltic" composition: $A = 10^{-6}$ Pa s, $B = 2.6 \times 10^4$ K, $T_m = 1220$ K. "Granitic" composition: $A = 10^{-7}$ Pa s, $B = 3 \times 10^4$ K, $T_m = 970$ K. Shown in parentheses is the corresponding melt viscosity at the onset of melting, $\eta_0 = A \exp(B/T_m)$.

that there is a critical Gruntfest number (or, equivalently, a critical thickness of the melt layer) that separates layers that gradually decelerate and freeze from those that ultimately result in thermal runaway [*Fialko*, 1999]. The Gruntfest number dictates whether the heat released by viscous dissipation is sufficient to offset the conductive losses to the ambient rocks, and prevent freezing. In case of a weakly supercritical Gn^*, equation (14) provides a lower bound on time required for the thermally-induced weakening.

Calculations illustrated in Figure 1 correspond to crystal-free equilibrium melts. The frictional melting during seismic slip may be selective and non-equilibrium, so that the effective melt rheology may substantially differ from equation (1) for a given composition of the host rock. For example, early fusion of the least refractory minerals such as biotite and amphibole in granite may give rise to melts of the essentially mafic composition [e.g, *Spray*, 1993]. However, if fusible minerals constitute only a small fraction of the total volume of the protolith, the shear strength of the partially molten gouge does not need to decrease, unless the low viscosity melt is efficiently segregated from the matrix into a continuous layer. If so, results shown in Figure 1 suggest that the silica-rich melts may not weaken on timescales that are small compared to typical rise times of earthquakes. The upper bound on the earthquake rise time is l/V_r, where l is the characteristic size of a slipping region, and V_r is the rupture velocity, so

that the rise times range from seconds for large earthquakes [*Kanamori and Anderson*, 1975] to milliseconds (or less) for micro-earthquakes. Thus small earthquakes are more vulnerable to the thermal arrest, especially if the ambient shear stress is low (e.g., in the shallow crust), and the frictionally-generated melts are rich in silica and poor in volatiles, rendering the effective viscosities in excess of $10^5 - 10^6$ Pa s [*McBirney*, 1993; *Rubin*, 1995].

2.2. Steady state shear under constant velocity

After the onset of thermal runaway, viscous resistance of the melt layer becomes negligible, and slip accelerates to a limiting velocity corresponding to the elastodynamic rupture with a nearly complete stress drop [*Freund*, 1998; *Fialko*, 2004a]. It is of interest to calculate the maximum melt temperature and the maximum thermal energy associated with such an end-member scenario. We seek a steady state solution to equation (2) corresponding to a constant slip velocity V_c. Noting that the local strain rate in the fluid is the across-flow gradient in melt velocity v, $\partial\epsilon/\partial t = \partial v/\partial x$, the steady state form of equation (2) is

$$\frac{d^2T}{dx^2} = -\frac{\tau}{k}\frac{dv}{dx}. \tag{15}$$

Integrating equation (15) with the boundary condition (8), we obtain

$$v = -\frac{k}{\tau}T', \tag{16}$$

where the prime operator denotes differentiation with respect to x, $T' = dT/dx$. Note that v is the fluid velocity relative to the center of the melt layer, so that $v(0) = 0$, and $v(\pm w) = \pm V_c/2$. Substituting equation (1) into equation (15), and eliminating the melt velocity using equation (16), one obtains the following expression for the melt temperature,

$$T'' = -\frac{\tau^2}{Ake^{B/T}}. \tag{17}$$

A joint solution of equations (17) and (16) is

$$v^2 = \frac{2kB}{A}\left[F\left(\frac{T_{max}}{B}\right) - F\left(\frac{T}{B}\right)\right], \tag{18}$$

where T_{max} is the maximum temperature at the center of the melt layer ($x = 0$), and

$$F(\xi) = \int \exp\left(-\frac{1}{\xi}\right) d\xi = \xi \exp\left(-\frac{1}{\xi}\right) + \mathrm{Ei}\left(-\frac{1}{\xi}\right), \tag{19}$$

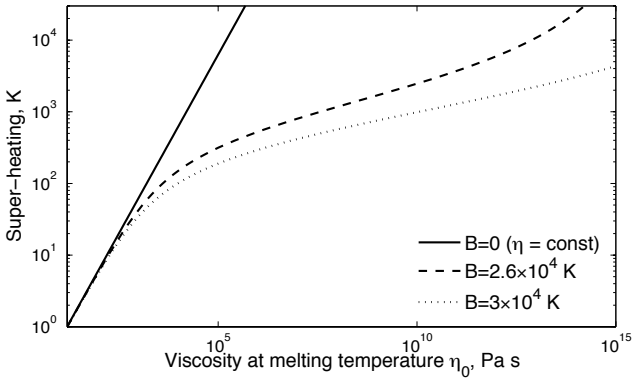

Figure 2. Maximum increases in the melt temperature at the center of the melt layer, for several values of the effective activation temperature B, and assuming slip velocity $V_c = 1$ m s^{-1}, and thermal conductivity k= 2 W K^{-1} m^{-1}.

Ei being the exponential integral, $\mathrm{Ei}(\xi)=\int_{-\infty}^{\xi} t^{-1}e^t dt$ [*Gradshteyn and Ryzhik*, 1994]. A somewhat simplified form of equation (18) can be obtained as follows,

$$\frac{v^2}{2k} = \int_T^{T_{max}} \frac{d\xi}{\eta(\xi)} = \frac{1}{\eta_0}\int_0^{T_{max}-T} d\xi \exp\left(\frac{B}{T_m} - \frac{B}{T+\xi}\right), \tag{20}$$

where $\eta_0 = \eta(T_m)$ the effective melt viscosity at solidus. From equation (20), the maximum overheating of melt with respect to solidus, $T_{max} - T_m$, corresponding to the slip velocity V_c is implicitly given by the following relation,

$$\frac{V_c^2}{8k} = \frac{1}{\eta_0}\int_0^{T_{max}-T_m} d\xi \exp\left(\frac{B}{T_m} - \frac{B}{T_m+\xi}\right). \tag{21}$$

In the limit of isoviscous melt ($B = 0$, $\eta_0 = A$), equation (20) reduces to

$$T(x) - T_m = \frac{V_c^2\eta_0}{8k}\left[1 - \left(\frac{x}{w}\right)^2\right]. \tag{22}$$

We point out that the steady state temperature due to shear heating is independent of the thickness of the melt layer. Figure 2 shows the maximum temperature increase, $T_{max}-T_m$, predicted by equations (18) and (21), as a function of the effective melt viscosity at solidus, $\eta_0 = A\exp(B/T_m)$, for a range of typical activation temperatures B. As one can see from Figure 2, the temperature dependence of melt viscosity severely limits the amount of energy dissipation on a fault surface. A strong negative feedback between the viscous heating and melt rheology practically prohibits coseismic temperature increases in excess of $\sim 10^3$ K, regardless of

the host rock composition and ambient stresses. The maximum temperature attainable on the fault surface scales with the initial melt viscosity, which in turn is primarily governed by the silica content. It follows that the generation of pseudotachylites in silicic rocks involves more thermal energy than in mafic protoliths. For mafic melts ($\eta_0 \sim 10^2 - 10^3$ Pa) the predicted post-melting temperature increase is only a few tens of degrees K for $V_c = 1$ m s^{-1} (Figure 2). The superheating of melt with respect to solidus is proportional to V_c^2 (equations (18) and (22)), so that an order of magnitude increase in the melt temperature would require increases in the fault slip velocity of about a factor of three. Note that in our estimates we use a slip velocity averaged over the rupture length. The local slip velocity may significantly exceed the average value (typically, of the order of a meter per second) near the rupture tips [e.g., *Fialko*, 2004a]. The near-tip peaks in slip velocity are highly transient, and thus not relevant to the quasi steady state conditions assumed in this subsection.

2.3. Viscoelastic effects

High slip velocities and localized deformation associated with earthquake ruptures imply high strain rates in the slip zone, and (if fusion occurs) in the eventual melt layer. This raises a question of the applicability limits of the assumption of a purely viscous deformation after the onset of melting. In particular, viscoelastic effects may become significant at strain rates that exceed a critical rate $\partial\epsilon_c/\partial t = K/\eta$, where K is an effective elastic modulus of melt at infinite frequency. The inverse of $\partial\epsilon_c/\partial t$ may be recognized as the Maxwell relaxation time for a viscoelastic material. Given that the loading strain rate is $\partial\epsilon/\partial t \sim O(V_c/w)$, a necessary condition for equation (3) to be applicable, $\partial\epsilon/\partial t < \partial\epsilon_c/\partial t$, may be written as

$$w > \frac{V_c \eta}{K}. \tag{23}$$

Using $V_c = 1$ m/s, $\eta = 10^6$ Pa s, and $K = 3$ GPa [e.g., *Webb and Dingwell*, 1990], equation (23) suggests that the viscous approximation (3) is valid for $w > 0.3$ mm. The latter condition is satisfied for most naturally observed pseudotachylites. The estimate (23) is likely conservative, as the effective melt viscosity at high ($\partial\epsilon/\partial t \gg 1$ s^{-1}) strain rates may decrease via the shear thinning mechanism [*Webb and Dingwell*, 1990], in addition (or prior) to the thermally-activated weakening.

3. Thermodynamics of frictional fusion

A strong coupling between the viscous deformation and heating of the melt layer implies that a full solution to a problem of frictional fusion must involve the consideration of phase transitions. Usually this is accomplished by introducing a Stefan-type boundary condition that relates jumps in the heat flux across the solid-liquid interface to the rate of solidification or freezing [*Landau*, 1951; *Huppert*, 1989; *Fialko and Rubin*, 1998, 1999; *Fialko*, 1999]. Because the earthquake slip zone has a finite thickness, and likely contains gouge particles with different melting temperatures, we account for the effects of partial melting of the gouge by introducing a new term in the energy balance equation,

$$\frac{\partial T}{\partial t} = \frac{\partial}{\partial x}\kappa(T)\frac{\partial T}{\partial x} + \frac{\tau}{c\rho}\frac{\partial \epsilon}{\partial t} - \frac{L}{c}\frac{\partial \phi}{\partial t}, \; t > 0, \; |x| < w \tag{24}$$

where L is the latent heat of fusion or crystallization, and ϕ is the volumetric melt fraction. The third term on the right-hand side of equation (24) represents the energy liberated or consumed in the result of phase transitions. Note that equation (24) also allows for the temperature dependence of the thermal diffusivity κ. We assume that $\kappa(T)$ is dominated by the temperature dependence of the thermal conductivity k,

$$k(T) = a + \frac{b}{77 + T}, \tag{25}$$

where $a = 1.18$ W K^{-1} m^{-1}, and $b = 474$ K are empirically determined constants [e.g., *Clauser and Huenges*, 2000]. Prior to melting, the rate of heat production (the second term on the right hand side of Equation (24)) is given by $\mu\sigma_n V_c/2wc\rho$, where μ is the coefficient of friction, σ_n is the normal stress resolved on the slip plane, $\tau = \mu\sigma_n$ is the Coulomb stress, and $\partial\epsilon/\partial t = V_c/2w$ is the strain rate. After melting is complete, the shear stress is governed by the Navier-Stokes relation (3). Given that the viscous stress must be constant across the melt layer, equation (3) may be integrated over the thickness of the layer, yielding

$$\tau = \frac{V_c}{\int_{-w}^{w} \frac{dx}{\eta(x)}}. \tag{26}$$

Note that for a temperature-dependent melt viscosity equation (3) implies a non-Newtonian melt rheology as the strain rate is allowed to vary across the melt layer proportional to a local viscosity.

The effective viscosity of a partially molten fault gouge depends not only on the melt temperature, but also on the clast content. We account for the effect

of solid inclusions using an empirically derived expression for polymer melts [*Kitano et al.*, 1981]. The corresponding modification of equation (1) gives rise to the following rheology,

$$\eta(T,\phi) = A\exp\left(\frac{B}{T}\right)\left(1-\frac{1-\phi}{1-\phi_0}\right)^{-2}, \qquad (27)$$

where ϕ_0 is the minimum melt fraction below which the viscous approximation is no longer valid. The rheology of a partially molten gouge is poorly known for small melt fractions, and we use the Coulomb stress to evaluate the frictional heating for $\phi < \phi_0$. The critical melt fraction ϕ_0 only weakly depends on the aspect ratio of solid inclusions, and we use an experimentally inferred value of $\phi_0 = 0.46$ [*Kitano et al.*, 1981] in all calculations below. The melt fraction ϕ is itself a function of temperature and lithology. When the rate of heating is sufficiently small the clast temperature is gradually brought to solidus and conditions for a local thermodynamic equilibrium are satisfied. In this case the melt fraction can be considered a simple (e.g., linear) function of temperature, such that $\phi(T_s) = 0$ and $\phi(T_l) = 1$, where T_s and T_l are solidus and liquidus, respectively.

3.1. Simulation of high-speed friction experiments

We test our model by simulating laboratory measurements of friction at sliding velocities of the order of 1 m s^{-1} [*Tsutsumi and Shimamoto*, 1997; *Hirose and Shimamoto*, 2003, 2005]. Although these experiments were conducted at low normal stresses of a few megapascals, macroscopic melting on the slip interface occurred about 10 seconds after the initiation of sliding. The condition of a local thermodynamic equilibrium requires that

$$t_h \gg \frac{a^2}{\kappa}\left(1+\frac{L}{c\Delta T}\right), \qquad (28)$$

where t_h is the heating time over which the average temperature of the gouge is raised to solidus, ΔT is the clast undercooling with respect to solidus, and a is the characteristic clast size. In the experiments of Hirose and Shimamoto the initial thickness of the melt layer is about 30 μm (and the clast size a is smaller still), so that the condition (28) is clearly satisfied. Therefore we conclude that for these experiments the assumption of a local thermodynamic equilibrium is valid. Note that the condition of a thermodynamic equilibrium (28) does not imply a chemical equilibrium between different mineral phases of the host rock, and the generation of the eutectic (minimum) melt.

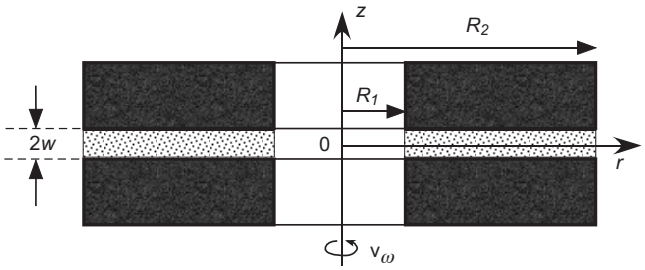

Figure 3. Configuration of the rotary shear experiments of *Hirose and Shimamoto* [2005]. The specimen consists of two coaxial thick-walled cylinders with inner and outer radii of R_1 and R_2, respectively. One cylinder is fixed, while the other is rotated at an angular velocity ω. The instantaneous thickness of the frictionally generated melt layer is $2w$.

The geometry of the experiment of *Hirose and Shimamoto* [2005] is shown in Figure 3. We consider the evolution of shear stresses on the slip interface in the viscous regime, i.e., after the onset of macroscopic melting. The fluid-mechanical part of the problem is governed by the Navier-Stokes equations [e.g., *Turcotte and Schubert*, 2002, p.237]. The problem has obvious symmetries about the slip plane ($z = 0$, Figure 3), as well as the rotation axis z. Because the specimen is unconfined, melt can escape from the slip surface in a radial direction, thereby decreasing w, and increasing the viscous stresses. This implies that all 3 components of the fluid velocity vector, $v_i = (v_r, v_z, v_\omega)$ are non-zero. The relative magnitudes of the fluid velocity components can be estimated from the local conservation of mass. Assuming that the melt is incompressible, conservation of mass requires that

$$V_s = \frac{1}{r}\int_{-w}^{w}\frac{\partial(rv_r)}{\partial r}dz, \qquad (29)$$

where $V_s = v_z|_{z=w} - v_z|_{z=-w}$ is the rate of thinning of the melt layer due to radial extrusion. In the rotary shear experiments, V_s represents the axial shortening velocity of a specimen. Dimensional analysis of the conservation of mass gives rise to the following relation between v_r and V_s, $\pi(R_2^2 - R_1^2)V_s \approx 4\pi R_2 w v_r$, where R_1 and R_2 are the inner and outer radii of the thick-walled cylinder (Figure 3), so that

$$v_r \approx \frac{R_2^2 - R_1^2}{2R_2 w}V_s \approx \frac{R_2}{2w}V_s \gg V_s. \qquad (30)$$

Estimate (30) was obtained assuming that most of the melt loss from the slip interface occurs through the

outer ($r = R_2$) outlet. This assumption stems from a larger circumference (and thus greater cross-sectional area for radial flow) at $r = R_2$, and is in agreement with observations (T. Hirose, personal communication, 2005), and our theoretical model (Appendix A). Note that $v_\omega \gg v_r$, i.e., the main viscous losses are due to the sample rotation. Although the axial shortening velocity V_s is negligible compared to the slip velocity v_ω, the former is important because it affects the thickness of the melt layer, and thus the shear stress, viscous dissipation, and the rate of melting at the solid-liquid interface ($z = \pm w$, Figure 3). Analytic solution that relates the shortening velocity V_s to the rate of rotation and the applied axial load is presented in Appendix A.

The heat transfer in our numerical experiments is modeled using a 1-D finite difference scheme. Results of our simulation are shown in Figure 4 along with the experimental data of *Hirose and Shimamoto* [2005]. To account for significant variations in the coefficient of friction (and the heat generation) prior to the macroscopic melting, we approximate the pre-melting coefficient of friction using a piece-wise linear fit (see black solid line in Figure 4). The onset of melting in the model occurs when the average temperature of the slip interface reaches the solidus temperature of gabbro. The transition between the effectively solid and liquid states of the partially molten slip zone is controlled by the following condition,

$$\frac{V_c}{\int_{-w}^{w} \frac{dx}{\eta(x)}} < \mu\sigma_n. \tag{31}$$

The left-hand side of inequality (31) is the viscous stress corresponding to the slip velocity V_c, effective melt viscosity η, and thickness of the melt layer $2w$ (equation (26)), and the right-hand side is the Coulomb stress that describes the frictional strength of the gouge layer in the absence of melting. Once the condition (31) is met, the apparent coefficient of friction (the ratio of shear to normal stress) is calculated by solving a time-dependent coupled heat transfer - fluid-mechanical problem using as algorithm described in Appendix B. As one can see from Figure 4, the onset of macroscopic melting predicted by our model is reasonably close to the observed one, albeit the theoretical prediction is somewhat advanced. An earlier onset of melting in the model compared to observations might be anticipated, as we assume that all work done against friction is converted into heat, and all heat loss is by conduction only. In reality, some fraction of the external work done on the specimen may be dissipated via non-thermal processes such as micro-fracture and communition. In addition, some fraction of the dissipated energy is removed by non-conductive mechanisms, such as the advective loss of hot gouge, convective cooling by the ambient air, and radiative heat transfer. All these mechanisms are estimated to be small compared to the conductive heat loss, and therefore we do not include them in our model. We also note that the model somewhat underpredicts the peak shear stress at the onset of melting. Given uncertainties in the assumed thermophysical parameters and the effective melt rheology, the agreement between the modeled and observed onset of melting is quite good. The dashed line in Figure 4 shows the predicted evolution of the apparent coefficient of friction in a purely viscous regime. The theoretical curve is shifted horizontally to compensate for an early onset of melting in the model, and facilitate the model comparison with observations in the viscous regime. The overall evolution, as well as the residual values of the modeled coefficient of friction are in a reasonable agreement with the experimental data. We point out that the magnitude of the residual shear stress in the post-melting stage is controlled by complex interactions between the shear heating and radial extrusion of melt, evolution of the clast content, melt thickness, etc., so that the agreement between the model and the experimental data in Figure 4 is encouraging. Our calculations also show that some complexity in the experimental data may be due to a non-uniform heating resulting from radial variations in slip velocity. For example, the second onset of strengthening (at displacement of $\sim$6 m, see Figure 4) begins when the temperature at the external boundary of the slip surface ($r = R_2$) reaches about 720 K. The strengthening continues as the 720 K isotherm propagates toward the inner boundary ($r = R_1$), and reaches a saturation level when the entire slip surface is heated above 720 K. Future experiments employing the rotary shear configuration may greatly benefit from the sample geometries that minimize spatial variations in the slip velocity (e.g., such that $R_2 - R_1 \ll R_1$).

3.2. Can non-equilibrium melting produce superheated pseudotachylites?

Theoretical considerations (Section 2) confirmed by detailed numerical experiments (Section 3.1) indicate that heating of the fault slip zone is most robust while the gouge layer is effectively solid. Immediately upon the transition to a viscous rheology the negative feedback between heating and viscosity efficiently buffers further increases in temperature (Figures 2 and 4). An important parameter governing the solid-liquid transition is the critical clast content $1 - \phi_0$ (see equa-

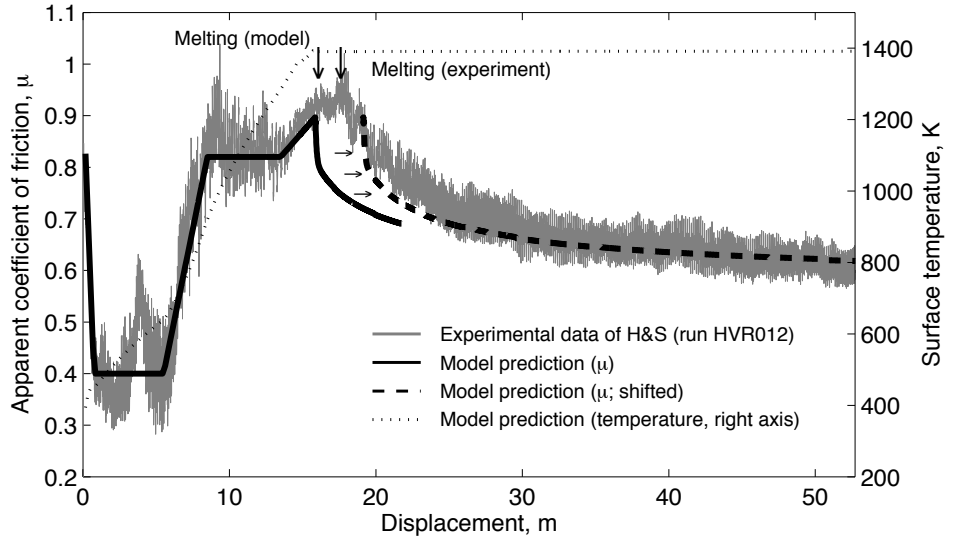

Figure 4. The effective coefficient of friction (ratio of shear and normal stresses) measured in high-speed friction experiments of *Hirose and Shimamoto* [2005] (light rugged line), and simulated using our numerical model (black lines). The dashed line denotes the calculated apparent coefficient of friction in the post-melting stage, shifted to account for the early onset of melting in simulations. The dotted line denotes the predicted average surface temperature of the specimen. The following parameters were used in numerical simulations: $R_1 = 7.5$ mm, $R_2 = 12.5$ mm, $v_\omega = 0.85$ m s^{-1}, $\sigma_n = 1.5$ MPa, $L = 5 \times 10^5$ J kg^{-1}, $A = 3 \times 10^{-7}$ Pa s, $B = 2.62 \times 10^4$ K.

tion (27)). As the melting degree reaches a value of ϕ_0 the effective viscosity drops dramatically, thereby reducing the heat generation, and further melting. We will refer to the equilibrium temperature that corresponds to the critical melt fraction ϕ_0 as to the effective lubrication temperature. Numerical simulations indicate that under the thermodynamic equilibrium conditions the melt fraction cannot be much larger than ϕ_0, and melt temperature may only slightly exceed the lubrication temperature (Figure 4). However, field observations show that the clast content in natural pseudotachylites can be significantly lower than $1 - \phi_0 \approx 50\%$, and melt superheating with respect to the effective solidus may be as large as a few hundred degrees [*Lin and Shimamoto*, 1998; *Otsuki et al.*, 2003; *Di Toro and Pennacchioni*, 2004]. For example, *Di Toro and Pennacchioni* [2004] describe pseudotachylite veins in the Adamello tonalites (Italian Southern Alps) that were presumably formed by seismic faulting in the middle crust at pressures of 250-300 MPa. The mineral composition of the host tonalite is as follows: 17% biotite, 6% K feldspar, 48% plagioclase An45, and 29% quartz [*Di Toro and Pennacchioni*, 2004]. If the frictional melting occurred under conditions of a thermodynamic equilibrium, one might expect a complete fusion of the less refractory biotite and potassic feldspar, and partial fusion of approximately half of plagioclase, so that the resudial clast content would be of the order of 50%. However, the total clast content in the Adamello pseudotachylites is as low as ∼15%, with more than 90% of plagioclase and almost 60% of quartz fused. Unless the refractory minerals are able to dissolve at temperatures well below the solidus in the postseismic period [e.g., *Knoche and Luth*, 1996], the observed low clast content seems to require an appreciable superheating of melt with respect to the lubrication temperature [*Di Toro and Pennacchioni*, 2004; *Lin and Shimamoto*, 1998]. Here we investigate a possibility that the inferred superheating might result from a non-equilibrium melting (hereafter referred to as "fast fusion") of the fault gouge material.

The fast fusion mechanism is based on a fact that the gouge particles have a finite size, and thus require a finite time to warm up and melt. Therefore at the initial stages of seismic slip, when the heating rate is high, there is a time lag between heating and melting. This time lag implies that the instantaneous clast content in the melt may be higher than that resulting from the equilibrium fusion. If so, the effective viscosity and the rate of thermal dissipation might remain high even at temperatures comparable to the melting point of the re-

fractory phases of the fault gouge (e.g., plagioclase and quartz in the granitic protolith), resulting in the temperature overshoot with respect to the lubrication temperature, and subsequent melting of a significant part of the refractory clasts. In order to quantify this effect, one needs to consider the details of heating, melting, and melt removal at the clast boundary.

The mechanical interaction between individual clasts during rapid shearing gives rise to a progressive heating of the clasts that proceeds from the clast surface (area of contact with other particles) into the clast interior. Thus the highest temperatures, and, eventually, melting, is expected to occur on the clast surface. Once a film of melt covers the clast surface, interaction with the adjacent clasts will result in squeezing and removal of melt from the area of contact between the adjacent particles. The film thinning will proceed until the viscous resistance to flow exceeds the driving stress. The residual film acts like a thermal boundary layer that controls the heat flux, and further melting of the clasts. We model the melt removal from a narrow gap between two clasts subject to the normal stress σ_n by considering the radial flow of melt between two co-axial disks having radius a that corresponds to the characteristic clast size. The rate of the clast convergence, $\partial w/\partial t$, can be estimated using the analytical solution presented in Appendix A (see equation (A16) for $\alpha = 0$, $C = 8$, and assuming that the dynamic viscosity η is constant),

$$\frac{\partial w}{\partial t} = -\frac{16 w^3 |\delta\sigma|}{3\eta a^2}, \tag{32}$$

where $\delta\sigma$ is the pressure drop that drives the melt extrusion. At the same time, melting tends to increase the thickness of the melt film, $2w$, between the clasts. Assuming that the temperature at the clast boundary is the melting temperature T_m, and the temperature gradient inside the clast is small compared to the temperature gradient $(T - T_m)/2w$ across the boundary layer, one can write the Stefan condition as follows,

$$\rho L \frac{\partial a}{\partial t} = -k \frac{T - T_m}{2w}. \tag{33}$$

Next, one can estimate the thickness of the quasi-stationary boundary layer, $2w$, by equating the squeezing velocity (32) to the melting velocity (33), $\partial w/\partial t = \partial a/\partial t$, which yields

$$2w = a^{1/2} \left(\frac{3}{2} \frac{\eta c (T - T_m)}{\delta\sigma L} \right)^{1/4}. \tag{34}$$

Equations (32) and (33) can be also used to determine the instantaneous rate of melting,

$$\frac{\partial a^{3/2}}{\partial t} = -\left(\frac{\delta\sigma}{\eta} \right)^{1/4} \left(\frac{3c(T - T_m)\kappa}{2L} \right)^{3/4}. \tag{35}$$

Particular values of the pressure drop $\delta\sigma$ are not well constrained, as the latter depends on details of the mechanical interaction between individual clasts. On average, $\delta\sigma$ is likely to be some fraction of the fault-normal stress σ_n. For simplicity, we assume $\delta\sigma = 10^{-2}\sigma_n$ in our simulations. Note that uncertainties in the actual value of the pressure drop should not significantly affect our estimates, as the residual melt thickness $2w$ (34) and the rate of clast melting (35) only weakly ($\propto \delta\sigma^{1/4}$) depend on the driving pressure drop. We also assume that the clasts are equidimensional, and the temperature of the clast interiors cannot exceed the effective solidus T_m until melting is complete.

Equation (35) may then be used to calculate the evolution of the clast content, shear stress, and temperature in the gouge layer during fast fusion. As an example, we present calculations for the pseudotachylite composition described by *Di Toro and Pennacchioni* [2004]. Figure 5 shows the model predictions for the initial thickness of the gouge layer of 10 mm, shear stress of 250 MPa, and various initial clast sizes. The melting begins when the temperature reaches the solidus of plagioclase (1520°K for An45; *Nekvasil and Burnham* [1987]). The viscosity of melt in the boundary layer is taken to be that of a pure anorthite melt [*Urbain et al.*, 1982],

$$\eta(T) = 7.4 \times 10^{-4} \exp\left(\frac{2.1909 \times 10^4}{T} \right), \tag{36}$$

and we assume that there is no melt loss from the fault surface (e.g., via melt fracturing). At every timestep, we track the clast content for every mineral phase present in the host tonalite. As one can see from Figure 5, survival of clasts during the initial stages of rapid heating is able to maintain the dissipation of heat up to temperatures as high as $1600 - 1700$°K, well beyond the melting point of the least refractory components. The predicted peak temperatures are higher still if one uses the effective solidus of plagioclase of 1700°K quoted by *Di Toro and Pennacchioni* [2004]. We conclude that fast fusion is a viable mechanism for generating superheated melts, and reducing the clast contest in pseudotachylites below the critical value of $1 - \phi_0 \approx 50\%$ (equation (27)). An interesting implication from this hypothesis is that the average size of clasts in the gouge layer prior to melting should inversely correlate with the clast content in the pseudotachylite. That is, clasts in

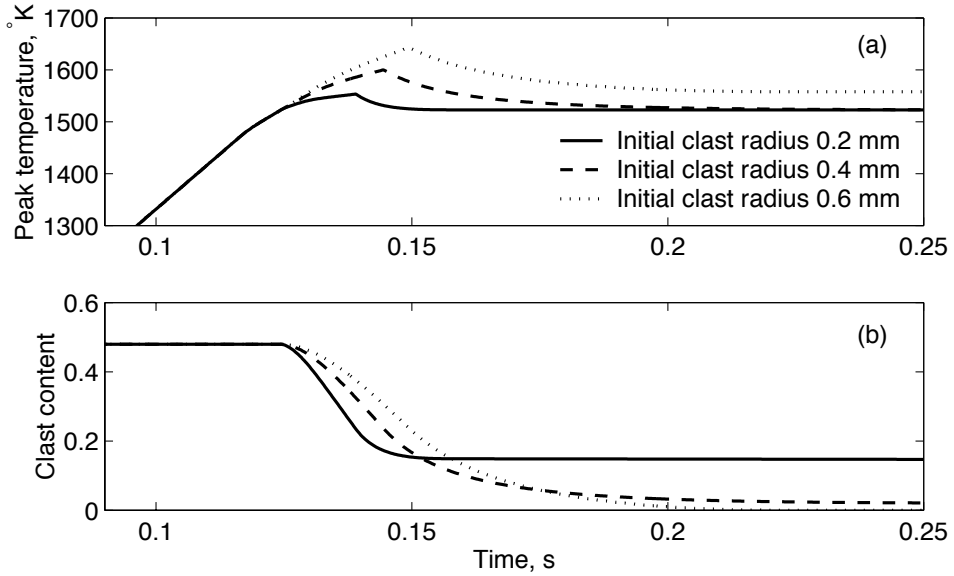

Figure 5. Evolution of (a) temperature and (b) content of the plagioclase (An45) clasts in a pseudotachylite of a tonalitic composition [*Di Toro and Pennacchioni*, 2004] due to fast fusion. Larger clasts give rise to a stronger temperature overshoot, and larger degrees of melting.

a coarse-grained gouge may have a lesser chance of survival after the onset of melting due to a greater tendency for the temperature overshoot.

4. Discussion

A complex dependence of friction on the amount of slip and slip velocity revealed by the high-speed friction experiments [e.g., Figure 4; *Tsutsumi and Shimamoto*, 1997; *Goldsby and Tullis*, 2002; *Hirose and Shimamoto*, 2003; *Di Toro et al.*, 2004; *Hirose and Shimamoto*, 2005] suggests that more than one mechanism may be responsible for the observed variations in the apparent kinetic friction. The high-speed laboratory data exhibit significant deviations from predictions of the rate and state model [*Dieterich*, 1979; *Ruina*, 1983]. It was proposed that the dramatic weakening observed at high slip velocities in several materials, including rocks and metals, may be due to "flash melting" of the contact asperities [*Bowden and Persson*, 1960; *Molinari et al.*, 1999; *Rice*, 1999], or perhaps some non-thermal mechanism such as the silica gel formation [*Di Toro et al.*, 2004]. The flash melting hypothesis postulates that the strength of asperities that support the shear stress resolved on a slipping interface is a decaying function of temperature, so that the frictionally generated heat weakens the asperities proportionally to a slip velocity. However, this hypothesis fails to explain an increase in the apparent friction prior to the onset of macroscopic melting [Figure 4; *Tsutsumi and Shimamoto*, 1997; *Hirose and Shimamoto*, 2005]. The silica gel mechanism does not seem to be applicable to the initial weakening observed in the silica-poor gabbroic rocks in experiments of *Tsutsumi and Shimamoto* [1997] and *Hirose and Shimamoto* [2005]. It should be noted that at least some fraction of the observed variations in the apparent friction (e.g., as seen in Figure 4) may be due to radial variations in slip velocity intrinsic to the rotary shear configuration (Figure 3). In particular, a higher slip rate further away from the axis of rotation implies an enhanced wear, and partial reduction in the normal stress on the sample periphery. This reduction must be compensated by an increase in the normal stress on the inner part of a cylindrical sample. The resulting migration of the load-bearing interface toward the internal radius of a sample must be accompanied by a decrease in the torque (or, equivalently, the apparent coefficient of friction) required to maintain a constant rotation velocity. Once some balance is established between the rates of slip and wear, the effective contact area, the torque, and the apparent coefficient of friction may return to their initial values. The effect of the loading configuration on the apparent friction may be verified, e.g., using samples having various internal (R_1) or external (R_2) radii.

If the pre-melting variations in the apparent friction are indicative of the intrinsic rock properties, and not the loading configuration, some explanation must be provided regarding the transient strengthening prior to the onset of macroscopic melting. One possibility is that the slip-strengthening may result from an increase in the effective contact area that offsets a thermally-induced decrease in the strength of individual asperities. Suppose that $F_n = \sigma_n S$ is the normal force applied to maintain the normal stress σ_n on a slip surface having area S. Also, suppose that $F_t = \tau_a S_a$ is the shear traction applied to produce slip on surface S, such that S_a is the total area of all contact asperities, and τ_a is the asperity strength. Provided that τ_a is a material property, the relative constancy of the coefficient of friction $\mu = F_t/F_n = \tau_a S_a/\sigma_n S$ over a wide range of normal stresses [*Byerlee*, 1978] implies that the actual contact area S_a is directly proportional to the applied normal stress, $S_a \propto \sigma_n$. This proportionality is likely due to brittle or plastic yielding of the asperities at high normal stress [e.g., *Bowden and Tabor*, 1954; *Teufel and Logan*, 1978],

$$\frac{S_a}{S} = \mu \frac{\sigma_n}{\tau_a}. \tag{37}$$

Assuming that τ_a approaches the theoretical strength of rocks (of the order of gigapascals; *Lawn* [1993, p. 12]), the actual contact area S_a comprises less than 10% of the total slip area S if the normal stress is of the order of 100 MPa (or less). Both yielding mechanisms that might operate on the asperity scale (i.e., plasticity and fracture) depend on temperature, so that τ_a is expected to decrease with slip, provided that the slip velocity is sufficiently high to raise the asperity temperature by several hundred degrees K. Such thermal weakening of the asperities may give rise to decreases in the coefficient of friction, provided that the thickness of a thermal boundary layer at the asperity contacts is small compared to the characteristic size of asperities, so that the contact area S_a remains relatively unaffected [e.g., *Bowden and Tabor*, 1954; *Bowden and Persson*, 1960]. However, continued slip and heating will eventually result in an enhanced asperity flattening, and increase in contact area S_a. Unless the asperity strength τ_a decays faster than S_a increases, the overall effect of temperature on μ may be slip-strengthening. The rock friction experiments conducted at low slip velocities, but high ambient temperatures confirm that the coefficient of friction increases with temperature [*Lockner et al.*, 1986; *Blanpied et al.*, 1995] (although some temperature weakening was reported for fluid-saturated quartz-rich rocks [*Chester*, 1994; *Blanpied et al.*, 1995]). Additional contribution to strengthening may be due to viscous shearing of intermittent films of melt generated at the asperity contacts [*Fialko*, 2004a; *Hirose and Shimamoto*, 2005].

While the details of evolution of the dynamic friction at the near-seismic slip velocities are still poorly understood, experimental data demonstrate that the initial transient decreases in friction are not sufficient to suppress further heating, and macroscopic melting. A major question is whether the pronounced increases in the effective coefficient of friction at the onset of macroscopic melting [Figure 4; *Tsutsumi and Shimamoto*, 1997; *Hirose and Shimamoto*, 2003] are capable of impeding or even terminating seismic slip. Our numerical simulations (see Section 3.1) indicate that the viscous braking is likely to become less efficient with the increasing depth. Several factors contribute to a reduced role of viscous braking at high confining pressures. First, the viscous resistance to slip is essentially independent of the fault-normal stress, while the static fault strength, and the absolute shear stress acting on a fault are expected to increase with depth. For a given melt rheology and thickness of the melt layer, there may be a characteristic depth below which the peak viscous stress is less than the driving shear stress (see equation (31)), which implies no strengthening at the onset of melting. Second, the characteristic time for the thermo-mechanical thinning of melt is inversely proportional to the square of the driving shear stress (equation (14) and Figure 1). Obviously, the efficiency of viscous braking is diminished if the timescale for the transient viscous strengthening is small compared to the earthquake rise time. Third, the high normal stresses imply that the effective area of the asperity contact S_a may not be small compared to the total slip area S (equation (37)). Small increases in the S_a/S ratio due to incipient melting may not be sufficient to offset the thermal weakening of the asperities, thereby preventing increases in the effective coefficient of friction.

Another question concerns the magnitude of the residual shear stress in the fully viscous regime. The apparent coefficient of friction associated with the post-melting slip in the rotary shear experiments of *Hirose and Shimamoto* [2005] is of the order of 0.5-0.6 (see Figure 4), i.e., comparable to the Mohr-Coulomb friction [*Byerlee*, 1978]. If the experimental data shown in Figure 4 were representative of seismic slip, one might conclude that earthquakes that produce pseudotachylites must have a low seismic efficiency, even when they occur in mafic host rocks. However, as discussed above, the apparent coefficient of friction has little meaning in the

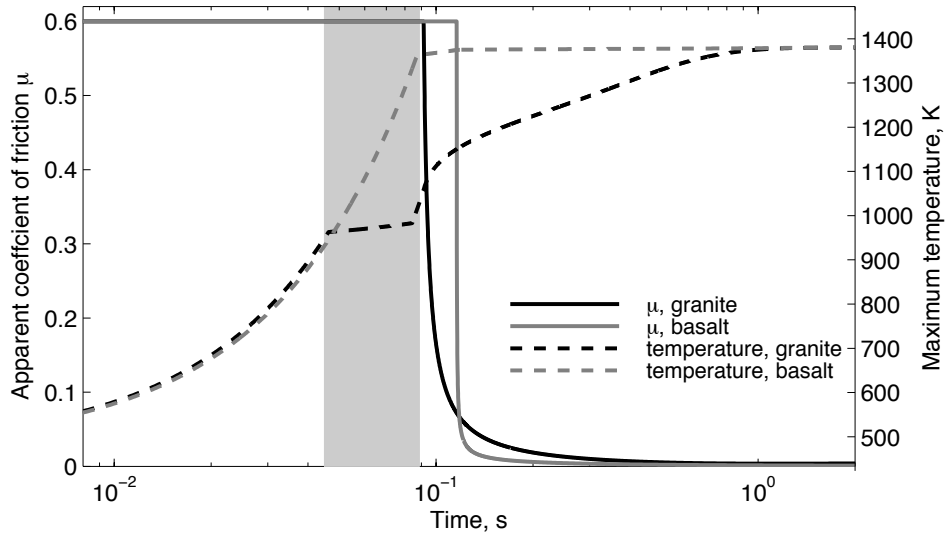

Figure 6. The effective coefficient of friction (solid lines) and the maximum temperature in the middle of the slip zone (dashed lines, right axis) for granitic and basaltic host rock compositions. The shaded area denotes an interval between the onset of melting, and the transition to the effectively viscous rheology in the model simulating slip in granite. This area represents a potential strengthening of the slip interface.

post-melting regime; in particular, it is expected to decrease with an increasing normal stress. To quantify the magnitude of the post-melting weakening under in situ conditions, we perform simulations of frictional heating and melting assuming the normal stress of 200 MPa, the effective pre-melting coefficient of friction of 0.6, slip velocity of 1 m s^{-1}, thickness of the slip zone of 5 mm, for the typical granitic and basaltic host rock compositions. We allow for the evacuation of melt from the slip surface, similar to that in the rotary shear experiments, to mimic the effect of the pseudotachylite vein injection. We assume an effective drainage distance (i.e., the characteristic vein spacing) of 1 meter. The pressure drop $\delta\sigma$ driving the melt withdrawal is of the order of the difference between the fault-normal stress σ_n, and the minimum compressive stress. For simplicity, we assume $\delta\sigma = 0.2\sigma_n$ in our calculations. Figure 6 illustrates the temporal evolution of the apparent coefficient of friction (solid lines) and the maximum fault temperature (dashed lines), for the granitic and basaltic rocks. In these simulations, the fault temperature reaches solidus within 0.1 s (i.e., after less than 10 cm of slip). The further temperature increase is temporarily buffered by the latent heat of melting. After melting proceeds beyond the critical melt fraction, the thermally induced melt thinning drastically reduces the shear stress to a new steady state value of the order of a few megapascals, rendering the effective coefficient of friction well below 0.1. Weakening associated with the transition to a viscous regime is accompanied by a localization of strain within the melt layer. The degree of localization is proportional to the slip velocity, but is essentially independent of the total amount of slip. For example, the basaltic melt layer having an initial thickness of 5 mm undergoes a localization of slip onto a shear zone as narrow as 0.1 mm. *Otsuki et al.* [2003] describe pseudotachylite layers having sub-millimeter thickness in well preserved fault zone rocks from the Nojima fault in Japan. The inferred strain localization in the viscous regime stems from the thermo-mechanical coupling and temperature dependence of the melt rheology, and has implications for the origin of pseudotachylites. In particular, it is commonly assumed that pseudotachylites form by melting on a sharp fault interface, and progressive widening of the melt layer via thermal erosion of the host rocks [e.g., *Jeffreys*, 1942; *McKenzie and Brune*, 1972]. Our results suggest an opposite scenario for the pseudotachylite formation, namely, the bulk melting of a slip layer having a finite thickness [*Cardwell et al.*, 1978; *Fialko*, 2004a], and the progressive localization of strain within the melt layer, depending on the initial layer thickness, and slip velocity. In fact, we find that it is quite difficult to increase the thickness of the melt layer once a transition to a viscous regime is complete.

An important corollary is that the observed thickness of the pseudotachylite layers represents the effective thickness of the seismic slip zone (upon appropriate corrections for the melt loss to the injection veins, postseismic melting due to overheating, etc.). Thus the apparent scaling of thickness of natural pseudotachylites with the inferred slip [*Sibson*, 1975; *Wenk et al.*, 2000] may be indicative of a correlation between the effective thickness of the earthquake rupture zone and the rupture length, rather than the progressive widening of a melt layer during seismic slip.

The low clast content, as well as the long injection veins observed in many natural pseudotachylites [e.g., *Lin and Shimamoto*, 1998; *Di Toro and Pennacchioni*, 2004] are direct evidence of high mobility of the frictionally-generated melts. These observations, along with theoretical arguments presented above indicate that the residual friction on faults with high-ϕ pseudotachylites must be small, and earthquakes that produced such pseudotachylites must have been accompanied by a nearly complete stress drop. At the same time, other pseudotachylites do not exhibit traits of significant viscous deformation [*Wenk et al.*, 2000], and thus might be evidence of a thermally arrested rupture. The velocity-strengthening behavior is most efficient at the stage of incipient melting (Figure 4), prompting a possibility that the lack of macroscopic melting on narrow fault zones that presumably produced earthquakes in the past [e.g., *Chester and Chester*, 1998] might be due to a self-limiting transition from the dry friction to the viscous rheology. Note that our numerical model explicitly precludes viscous braking; if the calculated resistance due to viscous shear is greater than the Mohr-Coulomb friction, the latter has been used to deduce the rate of heating within the slip zone. Our model may overestimate the tendency for the thermal runaway by preventing the migration of the slip zone in the fault-perpendicular direction, and enforcing shear of melt layers that might otherwise "stick", and eventually freeze. Shaded area in Figure 6 denotes a potential interval of viscous braking for the model simulating seismic slip in granitic rocks. Unfortunately, the defocusing of slip due to the transient viscous strengthening is hard to quantify. In addition, the magnitude of the viscous strengthening depends on the poorly known rheology of the partially molten gouge, especially at low degrees of melting. A transition from the viscous braking to the thermal runaway requires that the shear stress available to drive the slip must be sufficiently high to ensure the continued motion and heat generation in the partially molten layer, yet sufficiently low not to exceed the strength of the ambient rocks. An important parameter governing the efficiency of viscous braking is the effective thickness of the fault slip zone. First, the thickness of the slip zone directly controls the thickness of the melt layer, and thus the magnitude of the viscous stress (equation (3)). Second, the thickness of the slip zone w controls the temperature evolution along the earthquake fault [*Fialko*, 2004a]. In particular, faults that are thicker than the length scale for the thermal diffusion $\delta = \sqrt{\pi\kappa t}$ (e.g., $O(10^{-3}$-10^{-2} m) for the typical rise times $t \sim O$(seconds)) produce a nearly uniform increase in temperature along much of the fault length, implying a greater likelihood of thermal arrest in case of the thermally-induced strengthening. "Thin" ruptures ($w/\delta < 1$), on the other hand, may generate localized temperature increases near the rupture front [see, e.g., Figure 5a in *Fialko*, 2004a]. In this case, the transient strengthening associated with the incipient melting might be subdued by the high stress concentration at the rupture front (a scenario similar to the "direct effect" in the rate-and-state friction). Ultimately, studies of the effects of melting require coupling of the thermo- and fluid-dynamic aspects of high-speed friction (Sections 3.1-3.2) to the elasto-dynamic rupture simulations. Based on results of numerical experiments presented in this paper (Figures 1, 4, and 6), we conclude that the effects of viscous braking may be important for dry silicic rocks, particularly in the shallow upper crust, where the absolute shear stress may be relatively low (tens of megapascals). This conclusion may be supported by the apparent scarcity of pseudotachylites in quartz-rich rocks [e.g., *Sibson*, 1975; *Techmer et al.*, 1992], although the relative abundance of pseudotachylites in mafic and silicic rocks is not yet quantified. Systematic field studies are required to clarify the effect of the host rock composition on the likelihood of the pseudotachylite occurrence.

If the local stress conditions and the slip history are conducive to the occurrence of macroscopic melting, the intrinsic temperature-weakening of the frictionally generated melts will naturally limit the total amount of the energy dissipation on a fault. It was proposed that the anomalously low ratios of seismic energy to seismic moment observed for some earthquakes might be due to the enhanced thermal losses. For example, data from the 1994 Bolivian earthquake were interpreted as indicating significant ($10^3 - 10^5$ K, i.e., well above the liquidus) temperature increases on a fault surface [*Kanamori et al.*, 1998; *Bouchon and Ihmle*, 1999]. Results presented in Sections 2 and 3 (e.g., see Figures 2 and 6) suggest that the frictionally generated melts can-

not be strongly overheated, and thermal dissipation on a localized fault cannot be a significant sink of energy. Furthermore, the low residual strength of the supersolidus melt should give rise to a high seismic efficiency. It follows that the low energy to moment ratios cannot be explained in terms of frictional melting, and must be due to some other form of energy dissipation, e.g., that associated with fracture and damage in a finite volume around the earthquake slip zone. The anomalously low rupture velocity inferred for the Bolivian earthquake [*Beck et al.*, 1995; *Estabrook and Bock*, 1995] appears to be consistent with the latter interpretation.

Finally, we point out that large variations in the dynamic shear strength of the slipping interface associated with heating and melting imply large variations in the effective fracture energy, critical slip-weakening distance, and the dynamic stress drop. The modeling results shown in Figures 4 and 6 demonstrate that the residual dynamic friction, and the effective slip-weakening distance corresponding to the transition from dry friction to viscous flow are not material properties. In particular, they depend on the loading conditions (e.g., magnitude of stress and slip velocity), ambient temperature, host rock composition, etc. Therefore the residual friction, the critical weakening distance, and the effective fracture energy associated with the pseudotachylite-generating earthquakes may vary widely. Because the effective fracture energy scales with both the dynamic stress drop and the critical weakening distance, the fracture energy associated with earthquakes that give rise to macroscopic melting is likely to be much larger than the fracture energy associated with earthquakes that do not produce significant thermal weakening (due to melting, thermal pressurization, etc.) [e.g., *Abercrombie and Rice*, 2005].

5. Conclusions

We considered the evolution of the dynamic shear strength of a slip interface undergoing frictional melting. Our numerical model accounts for the frictional and viscous dissipation of heat in a sheared layer of a finite thickness, temperature-dependent heat conduction in the melt and the ambient solid, dependence of melt rheology on temperature and clast content, thermodynamics of phase transitions, and non-equilibrium melting of individual mineral phases in the assumed protolith (e.g., granite or gabbro). The model is used to simulate the high-speed rotary friction experiments of *Hirose and Shimamoto* [2005]. Given uncertainties in the assumed thermophysical parameters, the model predictions (in particular, the onset of melting, the residual magnitude of shear stress, and the rate of the melt extrusion from the slip surface) are in a good agreement with the laboratory data. We apply our model to infer the dynamics of frictional melting and viscous shear under in situ conditions corresponding to seismic faulting. A transition to the essentially viscous regime occurs when the melt fraction reaches a critical value of the order of 50%. This transition results in a dramatic drop in friction, and strain localization due to decreases in melt viscosity with increasing temperature (the so-called thermo-mechanical coupling, or thermal runaway). After the thermal runaway, the residual shear stress on a fault surface does not exceed a few megapascals, implying a nearly complete stress drop. A strong negative feedback between the effective melt viscosity, and dissipation of heat limits the maximum temperature attainable on the fault surface after the onset of melting. The maximum temperature is found to be close to that corresponding to 50% melting of the fault gouge. We propose that the low clast content, and substantial (a few hundred degrees) overheating with respect to the effective solidus inferred for some pseudotachylites may result from the non-equilibrium melting of clasts having a finite size (a process termed "fast fusion"). We propose that the temperature overshoot with respect to the effective solidus is inversely correlated with the average grain size in the fault gouge prior to melting. That is, a larger grain size implies a stronger temperature overshoot, and thus a reduced likelihood of the clast survival in the pseudotachylite. Our numerical simulations suggest that the dynamic shear strength of the partially molten gouge may exceed the Coulomb friction over a short interval corresponding to the evolution of melt fraction from zero to the critical value ($\sim 50\%$). A transition from viscous braking to lubrication occurs if the following three conditions are met: (i) the driving shear stress is sufficiently high to sustain slip despite viscous drag, (ii) there is no transfer of strain off of the fused fault surface, and (iii) the timescale for the thermal runaway is small compared to the duration of seismic slip. The timescale for the runaway is controlled by rheological properties of friction-generated melts, the content and composition of clasts, and the driving shear stress. Viscous braking should not appreciably affect the dynamics of shear rupture in mafic host rocks, but might be significant for silicic rocks, especially in the uppermost crust.

Acknowledgments. We thank Toshihiko Shimamoto and Takehiro Hirose for sharing results of their high-speed friction experiments, and providing insights about details

of the experimental runs. Very detailed and thoughtful reviews by two anonymous referees and the Associate Editor are greatly appreciated. This work was supported by NSF (grant EAR-0338061). Numerical codes used in this study are available from the authors.

Appendix A: Squeezing of melt from the rotary shear apparatus

We wish to evaluate the rate of axial shortening of the experimental sample due to the melt loss from the slip interface. This shortening results from squeezing of melt due to the applied axial force F. The dynamics of a thin melt layer at the sliding interface is governed by the Navier-Stokes equation,

$$\frac{\partial p}{\partial r} = \frac{\partial}{\partial z}\eta\frac{\partial v_r}{\partial z} + \rho\frac{v_\omega^2}{r}, \tag{A1}$$

where $\partial p/\partial r$ is the pressure gradient driving the radial flow. The second term on the right-hand side of equation (A1) represents a centripetal acceleration associated with the rotary motion v_ω. A dimensional analysis indicates that the ratio of the centripetal to the viscous term in equation (A1) is of the order of $\rho v_\omega^2 w^2/R_1\eta v_r \sim 10^{-2}-10^{-1}$ for the experimental parameters of *Hirose and Shimamoto* [2005], and we neglect the centripetal term in the following analysis. The solution to equation (A1) that satisfies the boundary conditions $v_r(\pm w) = 0$ (no slip at the walls), and $\partial v_r(0)/\partial z = 0$ (symmetry with respect to the middle of the melt layer) is

$$\frac{\partial v_r}{\partial z} = \frac{z}{\eta}\frac{\partial p}{\partial r}. \tag{A2}$$

Integration of equation (A2) yields

$$v_r = -\frac{\partial p}{\partial r}\int_z^w \frac{z}{\eta}dz. \tag{A3}$$

Because the rate of axial shortening V_s does not depend on the radial coordinate r, equation (29) provides a link between v_r and V_s,

$$\int_{-w}^{w} v_r dz = \frac{V_s r}{2} + \frac{b}{r}, \tag{A4}$$

where b is a constant of integration. The latter can be found by noting that the radial velocity v_r changes sign within the melt layer to allow melt squeezing at both the inner ($r = R_1$) and outer ($r = R_2$) outlets (Figure 3). This means that v_r must vanish at a certain radial distance R ($R_1 < R < R_2$),

$$\int_{-w}^{w} v_r dz = 0 \qquad \text{at} \quad r = R, \tag{A5}$$

so that equation (A4) gives rise to

$$\int_{-w}^{w} v_r dz = \frac{V_s}{2r}(r^2 - R^2). \tag{A6}$$

Combining equations (A3) and (A6), we obtain

$$\frac{V_s}{2r}(r^2 - R^2) = -\frac{\partial p}{\partial r}\int_{-w}^{w} dz\int_z^w \frac{y}{\eta}dy = -\frac{\partial p}{\partial r}\int_{-w}^{w}\frac{z^2}{\eta}dz = -\xi(r)\frac{\partial p}{\partial r}, \tag{A7}$$

where

$$\xi(r) = \int_{-w}^{w}\frac{z^2}{\eta}dz. \tag{A8}$$

Equation (A7) provides the following expression for the pressure gradient that drives the radial flow,

$$\frac{\partial p}{\partial r} = -\frac{V_s}{2r\xi(r)}(r^2 - R^2). \tag{A9}$$

Let us now assume that the melt pressure at the outlets is constant and equals to $p(R_1) = p(R_2) = p_0$ (e.g., atmospheric pressure in the laboratory experiments of Hirose and Shimamoto). By integrating equation (A9) with boundary condition $p(R_2) = p_0$, one obtains the following expression for the viscous pressure drop along the radial coordinate,

$$p(r) = p_0 + \frac{V_s}{2}\int_r^{R_2}\frac{r^2 - R^2}{r\xi(r)}dr. \tag{A10}$$

The unknown R can be found by satisfying the second boundary condition $p(R_1) = p_0$,

$$\int_{R_1}^{R_2}\frac{r^2 - R^2}{r\xi(r)}dr = 0. \tag{A11}$$

Integration of the viscous pressure drop (A10) over the contact area yields the following relationship for the applied axial force Φ,

$$\Phi = \pi p_0(R_2^2 - R_1^2) + \frac{V_s}{2}\int_{R_1}^{R_2} 2\pi r dr\int_r^{R_2}\frac{x^2 - R^2}{x\xi(x)}dx. \tag{A12}$$

Expressions (A10) and (A12) can be further simplified if one assumes that the melt viscosity η is independent of the radial coordinate. In this case,

$$R^2 = R_2^2\frac{1-\alpha^2}{2\ln(1/\alpha)}, \tag{A13}$$

where $\alpha = R_1/R_2$, and

$$p(r) = p_0 + \frac{V_s}{4\xi}\left(R_2^2 - r^2 - 2R^2\ln\frac{R_2}{r}\right), \tag{A14}$$

$$\Phi = \pi p_0(R_2^2 - R_1^2) + \frac{V_s}{4\xi}\int_{R_1}^{R_2} 2\pi r\left(R_2^2 - r^2 - 2R^2\ln\frac{R_2}{r}\right)dr. \tag{A15}$$

Finally, equation (A15) allows one to determine the velocity of the axial shortening due to melt squeezing out of the frictional interface as a function of the applied normal stress,

$$V_s = C\xi\frac{\sigma_n - p_0}{R_2^2}. \quad \text{(A16)}$$

In equation (A16), σ_n is the applied normal stress,

$$\sigma_n = \frac{\Phi}{\pi(R_2^2 - R_1^2)}, \quad \text{(A17)}$$

and C is the geometric factor,

$$C(\alpha,\beta) = \frac{8(1-\alpha^2)}{1+\alpha^4-\alpha^2-2\beta^2(1-\alpha^2+2\alpha^2\ln\alpha)}, \quad \text{(A18)}$$

where $\beta = R/R_2$. For the experimental configuration of *Hirose and Shimamoto* [2005], $\alpha = 0.6$. From equation (A13), this corresponds to $\beta \approx 0.79$. Equation (A16) allows one to calculate the axial shortening rate due to the melt extrusion V_s as a function of the applied force Φ, and the melt viscosity η.

Appendix B: Numerical scheme for simulations of partial melting at equilibrium conditions

We assume that the melt fraction $\phi(T)$ is a linear function of temperature in the interval $(T_s\ T_l)$, $\phi(T) = (T + T_l - 2T_s)/2(T_l - T_s)$, where $T_s = 1363$ K, and $T_l = 1383$ K are the assumed solidus and liquidus of gabbro, respectively. The 1-D computational domain spanning the melt layer consists of $N+1$ nodes x_i $(i = 0..N)$ such that $x_0 = -w$, $x_N = w$, and $\Delta x_i = x_{i+1} - x_i$. We solve equation (24) using a fully implicit finite difference scheme

$$\frac{T_i^{j+1} - T_i^j}{\Delta t} = \frac{2}{\Delta x_i + \Delta x_{i-1}}\left(\kappa_{i+1/2}\frac{T_{i+1}^{j+1} - T_i^{j+1}}{\Delta x_i} - \kappa_{i-1/2}\frac{T_i^{j+1} - T_{i-1}^{j+1}}{\Delta x_{i-1}}\right) - S(T_l - T_s)\frac{\phi_i^{j+1} - \phi_i^j}{\Delta t} + \frac{Q_i}{c\rho}, \quad \text{(B1)}$$

where $\Delta t = t^{j+1} - t^j$ is the time step, j is the timestep number, $\kappa_{i+1/2}$ and $\kappa_{i-1/2}$ denote the local thermal diffusivity averaged over the time steps $(t^{j+1} - t^j)$ and $(t^j - t^{j-1})$, respectively, $S = L/c(T_l - T_s)$ is the Stefan number, and $Q_i = \tau\partial\epsilon/\partial t$ is the rate of viscous heating. Equation (B1) is essentially non-linear as the thermal diffusivities $\kappa_{i+1/2}$, $\kappa_{i-1/2}$, the source term at the current time step Q_i, as well as the melt fraction at the next time step ϕ_i^{j+1} all depend on the unknown future temperature T_i^{j+1}. We solve equation (B1) using the following iterative procedure. At each time step we solve a system of linear equations generated by (B1) for T_i^{j+1}. In each iteration step the term representing the consumption or liberation of the latent heat $(\phi_i^{j+1} - \phi_i^j)/\Delta t$ is estimated based on the temperature values from the previous iteration. To suppress spurious oscillations and enhance convergence, we introduced the following predictor-corrector scheme,

$$L({}^{s+1}\phi(\bar{T}_i) - {}^{0}\ \phi(\bar{T}_i)) = c({}^{s+1}T_i - {}^{s+1}\ \bar{T}_i), \quad \text{(B2)}$$

where the left superscript s denotes the sequential iteration number, and $\bar{T}_i$ is the corrected temperature value. Iterations were continued until the relative change in temperature became smaller than a threshold value of 10^{-4}, $\max|{}^{s+1}T_i - {}^{s}\ T_i|/{}^{s+1}T_i < 10^{-4}$.

References

Abercrombie, R., and J. R. Rice, Can observations of earthquake scaling constrain slip weakening?, *Geophys. J. Int.*, *162*, 406–424, 2005.

Beck, S. L., P. Silver, T. C. Wallace, and D. James, Directivity analysis of the deep Bolivian earthquake of June 9, 1994, *Geophys. Res. Lett.*, *22*, 2257–2260, 1995.

Blanpied, M., T. Tullis, and J. Weeks, Frictional slip of granite at hydrothermal conditions, *J. Geophys. Res.*, *100*, 13,045–13,064, 1995.

Bouchon, M., and P. Ihmle, Stress drop and frictional heating during the 1994 deep Bolivia earthquake, *Geophys. Res. Lett.*, *26*, 3521–3524, 1999.

Bowden, F. B., and P. A. Persson, Deformation heating and melting of solids in high speed friction, *Proc. R. Soc. London, Ser. A*, *260*, 433–458, 1960.

Bowden, F. B., and D. Tabor, *The Friction and Lubrication of Solids*, Clarendon Press, Oxford, 1954.

Brodsky, E., and H. Kanamori, Elastohydrodynamic lubrication of faults, *J. Geophys. Res.*, *106*, 16,357–16,374, 2001.

Brune, J. N., T. Henyey, and R. Roy, Heat flow, stress, and rate of slip along San Andreas fault, California, *J. Geophys. Res.*, *74*, 3821–4009, 1969.

Byerlee, J., Friction of rock, *Pure Appl. Geophys.*, *116*, 615–626, 1978.

Cardwell, R., D. Chinn, G. Moore, and D. Turcotte, Frictional heating on a fault zone with finite thickness, *Geophys. J. Roy. Astron.*, *52*, 525–530, 1978.

Chester, F. M., Effects of temperature on friction - constitutive-equations and experiments with quartz gouge, *J. Geophys. Res.*, *99*, 7247–7261, 1994.

Chester, F. M., and J. S. Chester, Ultracataclasite structure and friction processes of the Punchbowl fault, San Andreas system, California, *Tectonophysics*, *295*, 199–221, 1998.

Clauser, C., and E. Huenges, Thermal conductivity of rocks and minerals, in *Rock physics and phase relations*, edited by T. J. Ahrens, pp. 105–126, AGU, Washington DC, 2000.

Di Toro, G., and G. Pennacchioni, Superheated friction-induced melts in zoned pseudotacylytes within the Adamello tonalites (Italian Southern Alps), *J. Struct. Geol.*, *26*, 1783–1801, 2004.

Di Toro, G., D. L. Goldsby, and T. E. Tullis, Friction falls towards zero in quartz rock as slip velocity approaches seismic rates, *Nature*, *427*, 436–439, 2004.

Dieterich, J. H., Modeling of rock friction 1. Experimental results and constitutive equations, *J. Geophys. Res.*, *84*, 2161–2168, 1979.

Dingwell, D., Melt viscosity and diffusion under elevated pressures, *Rev. Mineral.*, *37*, 397–424, 1998.

Estabrook, C. H., and G. Bock, Rupture history of the great Bolivian earthquake: slab interaction with the 660-km discontinuity?, *Geophys. Res. Lett.*, *22*, 2317–2320, 1995.

Fialko, Y., Time- and temperature-dependent evolution of stresses in a fault zone after the onset of frictional melting: Hints from numerical experiments, *Eos Trans. AGU Suppl.*, *80*, F682, 1999.

Fialko, Y., Temperature fields generated by the elastodynamic propagation of shear cracks in the Earth, *J. Geophys. Res.*, *109*, 10.1029/2003JB002,497, 2004a.

Fialko, Y., Probing the mechanical properties of seismically active crust with space geodesy: Study of the co-seismic deformation due to the 1992 M_w7.3 Landers (southern California) earthquake, *J. Geophys. Res.*, *109*, 10.1029/2003JB002,756, 2004b.

Fialko, Y., D. Sandwell, D. Agnew, M. Simons, P. Shearer, and B. Minster, Deformation on nearby faults induced by the 1999 Hector Mine earthquake, *Science*, *297*, 1858–1862, 2002.

Fialko, Y. A., and A. M. Rubin, Thermodynamics of lateral dike propagation: Implications for crustal accretion at slow-spreading mid-ocean ridges, *J. Geophys. Res.*, *103*, 2501–2514, 1998.

Fialko, Y. A., and A. M. Rubin, Thermal and mechanical aspects of magma emplacement in giant dike swarms, *J. Geophys. Res.*, *104*, 23,033–23,049, 1999.

Fleitout, L., and C. Froidevaux, Thermal and mechanical evolution of shear zones, *J. Struct. Geol.*, *2*, 159–164, 1980.

Freund, L. B., *Dynamic fracture mechanics*, 563 pp., Cambridge Univ. Press, New York, 1998.

Goldsby, D., and T. Tullis, Low frictional strength of quartz rocks at subseismic slip rates, *Geophys. Res. Lett.*, *29*, 10.1029/2002GL015,240, 2002.

Gradshteyn, I. S., and I. M. Ryzhik, *Table of integrals, series, and products*, 5th ed., 1204 pp., Academic Press, San Diego, 1994.

Gruntfest, I. J., J. P. Young, and N. L. Johnson, Temperatures generated by the flow of liquids in pipes, *J. Appl. Phys.*, *35*, 18–22, 1964.

Hirose, T., and T. Shimamoto, Fractal dimension of molten surfaces as a possible parameter to infer the slip-weakening distance of faults from natural pseudotachylytes, *J. Struct. Geol.*, *25*, 1569–1574, 2003.

Hirose, T., and T. Shimamoto, Growth of molten zone as a mechanism of slip weakening of simulated faults in gabbro during frictional melting, *J. Geophys. Res.*, *110*, B05,202, doi:10.1029/2004JB003,207, 2005.

Huppert, H. E., Phase changes following the initiation of a hot turbulent flow over a cold solid surface, *J. Fluid Mech.*, *198*, 293–319, 1989.

Jeffreys, H., On the mechanics of faulting, *Geol. Mag.*, *79*, 291–295, 1942.

Kanamori, H., and D. L. Anderson, Theoretical basis of some empirical relations in seismology, *Bull. Seis. Soc. Amer.*, *65*, 1073–1095, 1975.

Kanamori, H., and T. H. Heaton, Microscopic and macroscopic physics of earthquakes, in *Physics of Earthquakes, Geophysical Monograph, 106*, edited by J. Rundle, D. L. Turcotte, and W. Klein, pp. 117–136, AGU, Washington, DC, 2000.

Kanamori, H., T. H. Anderson, and T. H. Heaton, Frictional melting during the rupture of the 1994 Bolivian Earthquake, *Science*, *279*, 839–842, 1998.

Kitano, T., T. Kataoka, and T. Shirota, An empirical equation of the relative viscosity of polymer melts filled with various inorganic fillers, *Rheol. Acta*, *20*, 207–209, 1981.

Knoche, R., and R. Luth, Density measurements on melts at high pressure using the sink/float method: Limitations and possibilities, *Chem. Geol.*, *128*, 229–243, 1996.

Koizumi, Y., K. Otsuki, T. A, and H. Nagahama, Frictional melting can terminate seismic slips: Experimental results of stick-slips, *Geophys. Res. Lett.*, *31*, Art. No. L21,605, doi:10.1029/2004GL020,642, 2004.

Lachenbruch, A. H., Frictional heating, fluid pressure, and the resistance to fault motion, *J. Geophys. Res.*, *85*, 6097–6112, 1980.

Lachenbruch, A. H., and J. H. Sass, Heat flow and energetics of the San Andreas fault zone, *J. Geophys. Res.*, *85*, 6185–6222, 1980.

Landau, H. G., Heat conduction in a melting solid, *Q. Appl. Math.*, *8*, 81–94, 1951.

Lawn, B., *Fracture of Brittle Solids - Second Edition*, 378 pp., Cambridge University Press, Cambridge, 1993.

Lin, A., and T. Shimamoto, Selective melting process as inferred from experimentally generated pseudotachylytes, *J. Asian Earth Sci.*, *16*, 533–545, 1998.

Lockner, D. A., R. Summers, and J. Byerlee, Effects of temperature and sliding rate on frictional strength of granite, *Pure Appl. Geophys.*, *124*, 445–469, 1986.

Maddock, R., Frictional melting in landslide-generated frictionites (hyalomylonites) and fault-generated pseudotachylytes - discussion, *Tectonophysics*, *128*, 151–153, 1986.

Mase, C. W., and L. Smith, Effects of frictional heating on the thermal, hydrologic, and mechanical response of a fault, *J. Geophys. Res.*, *92*, 6249–6272, 1987.

McBirney, A., *Igneous petrology*, 2nd ed., 508 pp., Jones and Bartlett, Boston, 1993.

McKenzie, D., and J. N. Brune, Melting on fault planes during large earthquakes, *Royal Astron. Soc. Geophys. Jour.*, *29*, 65–78, 1972.

Molinari, A., Y. Estrin, and S. Mercier, Dependence of the coefficient of friction on the sliding conditions in the high velocity range, *J. Tribology*, *121*, 35–41, 1999.

Nekvasil, H., and C. Burnham, The calculated individual effects of pressure and water content on phase equilibria in the granite system, in *Magmatic processes: Physicochemical principles*, edited by B. Mysen, pp. 433–445, The Geochemical Society, Special Publication No. 1, University Park, PA, USA, 1987.

Otsuki, K., N. Monzawa, and T. Nagase, Fluidization and melting of fault gouge during seismic slip: Identification in the Nojima fault zone and implications for focal earthquake mechanisms, *J. Geophys. Res.*, *108*, 10.1029/2001JB001,711, 2003.

Philpotts, A. R., Origin of pseudotachylites, *Am. Jour. Sci.*, *262*, 1008–1035, 1964.

Price, N. J., Laws of rock behaviour in the earth's crust, in *Rock mechanics - Theory and practice*, edited by W. H. Somerton, pp. 1–23, Am. Inst. Mining and Metall. Engineers Symposium on Rock Mechanics, 11th, Berkeley, Calif., 1970.

Rice, J., Flash heating at asperity contacts and rate-dependent friction, *Eos Trans. AGU Suppl.*, *80*, F682, 1999.

Rubin, A. M., Propagation of magma-filled cracks, *Annu. Rev. Earth Planet. Sci.*, *23*, 287–336, 1995.

Ruina, A., Slip instability and state variable friction laws, *J. Geophys. Res.*, *88*, 10,359–10,370, 1983.

Scholz, C. H., *The mechanics of earthquakes and faulting*, 439 pp., Cambidge Univ. Press, New York, NY, 1990.

Shaw, H., Viscosities of magmatic silicate liquids: An empirical method of prediction, *Am. J. Sci.*, *272*, 870–893, 1972.

Sibson, R. H., Interaction between temperature and pore-fluid pressure during earthquake faulting - A mechanism for partial or total stress relief, *Nature*, *243*, 66–68, 1973.

Sibson, R. H., Generation of pseudotachylite by ancient seismic faulting, *Geophys. J. R. astr. Soc.*, *43*, 775–794, 1975.

Sibson, R. H., Thickness of the seismic slip zone, *Bull. Seism. Soc. Am.*, *93*, 1169–1178, 2003.

Spray, J. G., Viscosity determinations of come frictionally generated silicate melts-Implications for fault zone rheology at high-strain rates, *J. Geophys. Res.*, *98*, 8053–8068, 1993.

Spray, J. G., Evidence for melt lubrication during large earthquakes, *Geophys. Res. Lett.*, *32*, doi:10.1029/2004GL022,293, Art. No L07,301, 2005.

Suppe, J., *Principles of structural geology*, 537pp., Prentice-Hall, Englewood Cliffs, NJ, 1985.

Swanson, M. P., Fault structure, wear mechanisms and rupture processes in pseudotachylyte generation, *Tectonophysics*, *204*, 223–242, 1992.

Techmer, K., H. Ahrendt, and K. Weber, The development of pseudotachylyte in the ivrea-verbano zone of the italian alps, *Tectonophysics*, *204*, 307–322, 1992.

Teufel, L. W., and J. M. Logan, Effect of shortening rate on the real area of contact and temperature generated during frictional sliding, *Pure Appl. Geophys.*, *116*, 840–865, 1978.

Tsutsumi, A., and T. Shimamoto, High-velocity frictional properties of gabbro, *Geophys. Res. Lett.*, *24*, 699–702, 1997.

Turcotte, D. L., and G. Schubert, *Geodynamics, 2nd ed.*, 456 pp., Cambridge Univ., New York, NY, 2002.

Urbain, G., Y. Bottinga, and P. Richet, Viscosity of liquid silica, silicates and alumino-silicates, *Geochim. Cosmochim. Acta*, *46*, 1061–1072, 1982.

Wallace, R. C., Partial fusion along the Alpine Fault Zone, New Zealand, *Geological Society of America Bulletin*, *87*, 1225–1228, 1976.

Webb, S. L., and D. B. Dingwell, Non-Newtonian rheology of igneous melts at high stresses and strain rates - Experimental results for rhyolite, andesite, basalt, and nephelinite, *J. Geophys. Res.*, *95*, 15,695–15,701, 1990.

Wenk, H.-R., L. Johnson, and L. Ratschbacher, Pseudotachylites in the Eastern Peninsular Ranges of California, *Tectonophysics*, *321*, 253–277, 2000.

Yuen, D., L. Fleitout, G. Schubert, and C. Froidevaux, Shear deformation zones along major transform faults and subducting slabs, *Geophys. J. R. Astron. Soc.*, *54*, 93–119, 1978.

Y. Fialko and Y. Khazan, Institute of Geophysics and Planetary Physics, Scripps Institution of Oceanography, University of California San Diego, La Jolla, CA 92093. (e-mail: yfialko@ucsd.edu)

Received 6 June 2005; revised 6 September 2005; accepted 15 September 2005.